



Kahramanmaraş Sutcu Imam University

Journal of Engineering Sciences



Geliş Tarihi : 07.08.2023

Kabul Tarihi : 05.10.2023

Received Date : 07.08.2023

Accepted Date : 05.10.2023

INVESTIGATING CUTTING FORCE AND CUTTING POWER WHEN TURNING AA6082-T4 ALLOY AT CUTTING DEPTHS SMALLER THAN TOOL NOSE RADIUS

AA6082-T4 ALAŞIMININ TAKIM BURUN YARIÇAPINDAN DAHA KÜÇÜK KESME DERİNLİKLERİİNDE TORNALANMASINDA KESME KUVVETİ VE KESME GÜCÜNÜN ARAŞTIRILMASI

Kutay AYDIN¹ (ORCID: 0000-0003-3614-4877)

¹ Amasya University, Department of Mechanical Engineering, Amasya, Türkiye

*Sorumlu Yazar / Corresponding Author: Kutay AYDIN, kutay.aydin@amasya.edu.tr

ABSTRACT

Aluminum alloys are widely preferred engineering materials in the manufacturing industry due to their high formability, good mechanical strength, and low density. Machining problems in aluminum alloys include built-up-edge formation, chip rupturing, and low surface quality, particularly in the 6xxx series due to the high Si content in the machining area. The aim of this study was to investigate the influence of cutting depth smaller than the tool corner radius, and various cutting parameters on cutting force and cutting power in machining AA6082-T4 alloy. In this context, the Johnson-Cook material model was established for AA6082-T4 alloy, and machining behaviors in terms of cutting force, and cutting power were investigated by performing finite element method (FEM) analyses using a full factorial design and variance analyses with different machining parameters. In conclusion, the lowest cutting forces were achieved with a cutting depth of 0.3 mm and a feed of 0.1 mm/rev, and the lowest cutting power was obtained with a cutting speed of 300 m/min, a cutting depth of 0.3 mm, and a feed of 0.1 mm/rev. In addition, the most effective machining parameters have been determined as cutting depth with a ratio of 91.74% for cutting force and cutting speed with a ratio of 33.13% for cutting power based on the results of variance and regression analysis.

Keywords: Turning, AA6082-T4, finite element method, cutting forces, cutting power, corner radius

ÖZET

Alüminyum alaşımalar, düşük özgül ağırlık, iyi mekanik dayanım, yüksek şekillenebilme kabiliyeti vb. özelliklere sahip olmaları sebebiyle endüstride çok tercih edilen mühendislik malzemeleri arasındadır. Alüminyum alaşımın genelinde yiğintı talaş oluşumu ve 6xxx serisi için ise Si içeriği sebebiyle talaş kaldırma bölgesinde yırtılma ve kötü yüzey kalitesi problemleri, işleme sorunları olarak bilinmektedir. Bu çalışmada, AA6082-T4 alaşım için takım üç yarıçapından daha küçük kesme derinlikleri ve farklı işleme parametrelerinin kesme kuvveti ve kesme gücü üzerindeki etkilerine odaklanılmıştır. Bu kapsamda, AA6082-T4 alaşım için Johnson-Cook malzeme modeli kurulmuş ve farklı işleme parametreleri ile tam faktöriyel olarak sonlu eleman metodu (FEM) ve varyans analizleri yapılarak kesme kuvveti ve kesme gücü açılarından işleme davranışları incelenmiştir. Sonuç olarak; 0,3 mm kesme derinliği ve 0,1 mm/dev ilerleme miktarında en düşük kesme kuvvetleri, 300 m/dk kesme hızı, 0,3 mm kesme derinliği ve 0,1 mm/dev ilerleme miktarında ise en düşük kesme gücü elde edilmiştir. Buna ek olarak en etkili işleme parametrelerinin, kesme kuvveti için %91,74 oranla kesme derinliği ve kesme gücü için %33,13 oranla kesme hızı olduğu sonuçlarına ulaşılmıştır.

Anahtar Kelimeler: Tornalama, AA6082-T4, sonlu eleman metodu, kesme kuvvetleri, kesme gücü, üç yarıçapı

INTRODUCTION

Aluminum alloys are among the most preferred engineering materials in many industries such as aviation, automotive, electronics, manufacturing, etc., owing to their lightweight, high durability, and high resistance to oxidation (Torić et al., 2017; Mazzolani, 1994). In addition, 6xxx series aluminum alloys are used as a structural alloy by being accepted as an alternative to traditional structural steels due to their high strength at normal temperatures (Eurocode, 2007; Spigarelli, Evangelista, and McQueen, 2003). Although the machinability of aluminum alloys heat treated with tempering, surface hardening, etc. increases, negative properties such as rapid crack propagation and tearing in the chip removal zone adversely affect the machinability of silicon-containing alloys such as the 6xxx series (Yağmur, Kaya, and Şeker, 2021). Poor surface quality problems caused by built-up-edge formation in aluminum alloys are also known. Choosing a cutting depth smaller than the tool corner radius to improve the surface quality is a technique used in turning and micro-turning operations (Hasçelik and Aslantaş, 2021). Few studies have been found in the literature on the machining of AA6082-T4 alloy and its analysis by the finite element method. Yağmur et al. examined the effect of chip breaker forms on surface quality and cutting forces by processing AA6082-T4 alloy with polycrystalline diamond (PCD) insert. They measured the lowest cutting forces with inserts having a chip breaker. They obtained the best surface quality with the inserts without chip breaker and achieved more advantageous results as the cutting depth decreased in the inserts with chip breaker (Yağmur et al., 2021; Yağmur, Kaya, and Şeker, 2019). Stanojkovic and Radovanovic made a selection of end mills using the multiple criteria decision approach in the milling of AA6082-T4 alloy. The choice of cutting tool was made based on factors such as the number of cutting edges, cutting speed, feed rate, and cost criteria (Stanojković and Radovanović, 2017). Campatelli and Scippa studied the effect of different cutting parameters on cutting forces during milling of AA6082-T4 alloy and created a prediction model (Campatelli and Scippa, 2012). Borvik et al., using AA6082-T4 target plates, examined the effect of different tilt angles on the ballistic impact effect with experimental and FEM analyses. In terms of validating the FEM analyses with experimental findings, they obtained compatible results with APM2 type bullets, while lower validation rates were obtained with soft spherical core bullets (Børvik, Olovsson, Dey, and Langseth, 2011). El-Danaf et al. studied the hot forming ability of AA6082-T4 alloy. In this context, as a result of their experiments at various temperatures and strain rates, they observed that the ductility improved at high temperature and medium-speed strain rate conditions (El-Danaf, AlMajid, and Soliman, 2008). In the literature, it is seen that statistical and numerical analyses are widely used in addition to conventional experimental studies. Thanks to these methods, a significant saving in time and cost is obtained. In addition, these methods validate and support experimental studies and play a major role in determining solution sensitivity, effective parameters, and positive and negative factors on the problem (Shetty, Kumar, Mallagi, and Keni, 2021; Bolar, Das, and Joshi, 2018; Yilmaz, Dilipak, Sarıkaya, Yılmaz, and Özdemir, 2014). In many studies, analysis of variance (ANOVA), finite element method (FEM), linear and multiple regression models, Taguchi, ANN (artificial neural networks) and RSM (response surface method) methods were preferred (Yadav, 2021; Çiftçi and Gökçe, 2019; Davoudinejad, Doagou-Rad, and Tosello, 2018; Hazır, Erdinler, and Koc, 2018; Kumar, 2018; Chandrasekaran and Payton, 2013).

In this study, the effects of cutting depth smaller than the tool corner radius, and different machining parameters on cutting force and cutting power when turning AA6082-T4 alloy with PCD inserts were studied numerically. Regarding this matter, experimental data in a similar early study (Yağmur et al., 2021) were used to validate FEM analysis. Then, by selecting different tool geometry and machining parameters, FEM simulations, variance and regression analyses were made, and machining behaviors were examined in terms of cutting force and cutting power. Furthermore, a Johnson-Cook constitutive model was developed for AA6082-T4 alloy, which can be used in future machining studies.

METHODOLOGY

In the study, AA6082-T4 alloy was used as work material. Material composition of work material is given in Table 1, and its mechanical and physical properties are demonstrated in Table 2. The CCGW 09 T312 ISO coded insert without chip breaker from the tool manufacturer Diamond Tooling Systems (DTS) was used as a cutting tool. The material for the cutting tool was selected as polycrystalline diamond (PCD).

Machining parameters were referenced from the tool manufacturer's recommended range of cutting conditions for aluminum alloys (DTS). In the analysis, an insert with a tool corner radius of 1.2 mm was used and three independent factors (cutting depth, cutting speed and feed) with different levels were determined. The cutting depth levels were created with 25%, 50%, and 75% of the tool corner radius. The independent factors and levels for both cutting tools

are shown in Table 3. Tool rake angles, tool holder and positioning were kept constant for all machining conditions (Fig. 1).

Table 1. Material Composition of AA6082-T4 Alloy

% weight	Base	Si	Mg	Mn	Fe	Zn	Cr
AA6082-T4	Al	0.95	0.75	0.5	0.5	0.1	0.1

Table 2. Mechanical and Physical Properties of AA6082-T4 Alloy

Property	Value
Thermal conductivity (W/mK)	160
Specific heat (J/kgK)	900
Coefficient of thermal expansion (1/°C)	2.3E-5
Density (kg/m ³)	2700
Young's modulus (GPa)	70
Poisson ratio	0.33
Tensile strength (MPa)	260
Hardness (Brinel)	70

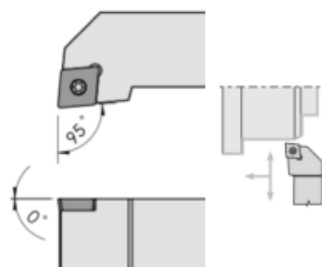


Figure 1. Tool Holder and Positioning

Although it is achievable to determine best machining conditions with cutting force data, variance and regression analyses were performed to obtain more detailed data. Minitab® R19 software was used for statistical analysis. Statistical analyses were performed using a full factorial design with selected control factors and levels (Table 3). Percent contributions and significance of each independent control factor and levels on the responses were obtained by analysis of variance. With the regression analysis, the empirical equation of the statistical model was established.

Table 3. Control Factors, Levels and Responses

Factors	Cutting Depth, a_p (mm)	Cutting speed, v (m/min)	Feed, f (mm/rev)
Level 1	0.3	300	0.1
Level 2	0.6	600	0.2
Level 3	0.9	900	
Responses	Cutting forces (N) Cutting power (W)		

Finite Element Method (FEM)

The finite element analyses were conducted using Third Wave AdvantEdge™ FEM software which was specialized for machining simulations. Updated-Lagrangian approach and adaptive remeshing technique were used in the simulations (Uğur, Kazan, and Özlu, 2022). The mesh structure of work material and cutting tool are formed with 4 nodes and 12 degrees of freedom elements. In numerical solutions in machining, deformation formation owing to temperature change and high stress and strain rate occur on the work material (Uğur, 2022; Ozlu and Uğur, 2021). In order to describe the stress-strain behavior of work material with high accuracy, material models based on hardening, strain rate and temperature change should be used (Gurusamy and Sriram, 2022; Rao, Dandekar, and Shin, 2011). For this reason, the Johnson-Cook constitutive model was used to describe the mechanical behavior of AA6082-T4 alloy. The Johnson-Cook constitutive model is expressed in Eq 1.

$$\sigma = \underbrace{[A + B\varepsilon^n]}_{\text{Elasto-Plastic}} \underbrace{\left[1 + C \ln\left(\frac{\dot{\varepsilon}}{\dot{\varepsilon}_0}\right)\right]}_{\text{Viscosity}} \underbrace{\left[1 - \left(\frac{T - T_{room}}{T_{melt} - T_{room}}\right)^m\right]}_{\text{Thermal Softening}} \quad (1)$$

Here; σ is flow stress, ε is plastic strain, $\dot{\varepsilon}$ is strain rate, and $\dot{\varepsilon}_0$ is reference strain rate. T is temperature, T_{melt} is melting point of the AA6082-T4 alloy, and T_{room} is room temperature. The constants of work material: A , B , C , n and m are initial yield stress, hardening modulus (coefficient of strain hardening), strain rate dependency coefficient, work hardening exponent, and coefficient of thermal softening, respectively. Since there are very limited studies on FEM analysis with AA6082-T4 alloy in the literature, some of the Johnson-Cook material model parameters were obtained from AA6082-T6 alloy and some by calculation. The m and C coefficients were used from the study of Jaspers and Dautzenberg (2002) with AA6082-T6 alloy. The n and $\dot{\varepsilon}_0$ coefficients were taken as reference from the study of Børvik et al. (2011) with AA6082-T4 alloy. The hardening modulus was calculated with the Hollomon equation. The ε_p plastic strain ratio required for the calculation was obtained as 0.0383 from the study of Karahan et al. (2017). The Hollomon equation, which expresses the power law relationship between plastic strain ratio and stress, is expressed in Eq. 2. The Johnson-Cook material model parameters are given in Table 4.

$$\sigma = K\varepsilon_p^n \quad (2)$$

Table 4. Johnson-Cook Parameters used for AA6082-T4 Alloy

Parameter	A (MPa)	B (MPa)	n	T_{melt} (°C)	T_{room} (°C)	m	C	$\dot{\varepsilon}_0$ (1/s)
Value	170	545.2	0.227	620	20	1.31	0.00747	5.0E-4

Third Wave AdvantEdge™ software uses the Coulomb friction model which is expressed in Equation 3. In the equation, the frictional force, friction coefficient and the normal force are F_f , μ , and F_n , respectively. In FEM analysis, the friction coefficient between aluminum alloys and PCD material was determined as 0.27 from early studies (Davim et al., 2010; Davim, Maranhao, Jackson, Cabral, and Gracio, 2008).

$$F_f = \mu F_n \quad (3)$$

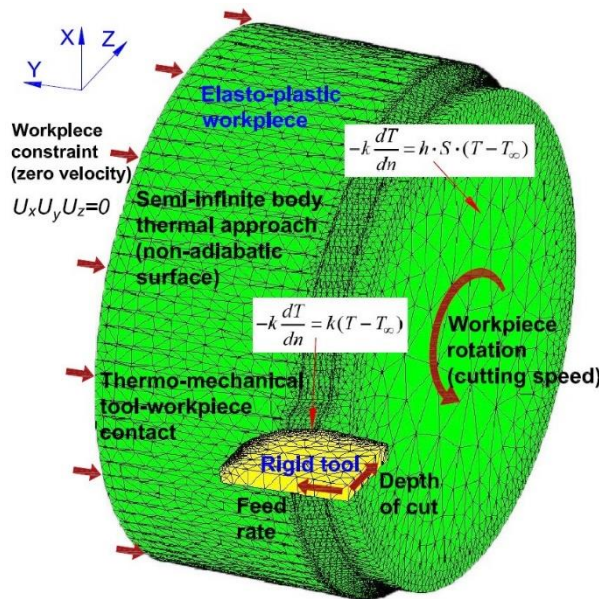
In FEM analysis, mesh structure is an important factor affecting the accuracy of the analysis, as well as the definition of the work material and the friction model. In machining simulations, it is critical that the minimum mesh element size is at least half the feed. In addition, very small minimum mesh size increases the simulation time (AdvantEdge, 2015). The cutting tool, work material and other mesh parameters are shown in Table 5. The rigid tool moves were defined horizontally on the positive Y-axis as feed. The elasto-plastic work material was fixed at zero velocity on the X-Y-Z axes. The work material was only moved rotationally counterclockwise on the Y-axis as cutting speed. In Fig. 2, all boundary conditions and the mesh structure of the finite element model are presented.

Validation of FEM Analyzes

Validation and verification of FEM analyzes were achieved with experimental findings referenced from early study including the machining of AA6082-T4 alloy with cutting tools of similar geometric design (Yağmur et al., 2021). For verification; cutting force measurements (Table 7) obtained with cutting parameters of 0.8 mm tool corner radius, 0.26 mm cutting depth, 0.14 mm/rev feed, and 400 m/min cutting speed were compared with FEM analyses to verify the FEM model and select appropriate mesh parameters. FEM analyses were performed for the experimental force measurement by selecting different mesh parameters (Table 6). In Table 6, error percentages and relative difference percentages were calculated to compare the FEM cutting force with the experimental cutting force. The error values represent the error between the FEM cutting force and the experimental cutting force in percentage. The relative difference values express in percentage terms how much the FEM cutting force differs compared to the FEM cutting force in the previous row. When the relative difference is small enough, it indicates that a fine enough mesh structure has been reached. The error percentage increases when lower-precision elements are created during mesh regeneration. Furthermore, the error percentage increases significantly when the minimum element size of the work material and cutting tool are increased.

Table 5. Mesh Structure Parameters

Initial cutting tool mesh	Value
Element size (max)	0.3 mm
Element size (min)	0.03 mm
Grading of mesh	0.5
Safety of curvature	1.5
Segments per edge	0.5
Min. element edge length	0.0002 mm
Initial work material mesh	
Work material diameter	6 mm
Work material length	3 mm
Element size (max)	3 mm
Element size (min)	0.05 mm
Grading of mesh	0.5
Safety of curvature	2.5
Segments per edge	2.5
Chip bulk	0.07475 mm
Cutter edge	0.05717 mm
Adaptive mesh refinement	
Refinement factor of mesh	20 (max-fine)
Coarsening factor of mesh	1 (max-fine)
Refinement factor of chip	3 (max-refine)
Grading near cutting edge	6
Factor of grading radius	4

**Figure 2.** Boundary Conditions and Mesh of the Finite Element Model

By selecting the parameters of 0.03 mm for the minimum element size of the work material, 0.05 mm for the minimum element size of the cutting tool, refinement factor of mesh of 20 (20 max. fine 1 max coarse), and coarsening factor of mesh of 1 (1 max. fine - 20 max. coarse), the lowest error percentage of 8.82% and a small relative difference percentage were obtained. Therefore, FEM analyses were conducted with these mesh parameters. For validation; cutting force measurements in some machining parameters in early study (Yağmur et al., 2021) and cutting force measurements obtained from FEM analyzes were compared. These comparison data is shown in Table 7. In the “Validation ratio” column, the ratios of the cutting forces obtained from the experimental and FEM analyzes to each other are expressed as percentages. In all FEM analyses, validation ratios of over 90% were obtained. According to early studies, it was determined that the validation ratios obtained were consistent and adequate (Gao, Wu, Zhang, and Luo, 2013; Mamedov and Lazoglu, 2013; Dandekar, Shin, and Barnes, 2010).

Table 6. Verification of FEM Model

Work material min element size (mm)	Cutting tool min element size (mm)	Refinement factor of mesh	Coarsening factor of mesh	Cutting force FEM (N)	Cutting force Experimental (Yağmur et al., 2021) (N)	Error (%)	Relative difference (%)
10	0.05	20	1	149.28	77.96	47.78	-
5	0.05	20	1	137.14	77.96	43.15	8.85
3	0.05	20	1	126.33	77.96	38.29	8.56
0.03	0.3	20	1	115.49	77.96	32.50	9.39
0.03	0.1	20	1	102.63	77.96	24.04	12.53
1	0.05	20	1	90.21	77.96	13.58	13.77
0.03	0.05	20	10	89.18	77.96	12.58	1.15
0.5	0.05	20	1	88.85	77.96	12.26	0.37
0.1	0.05	20	1	87.73	77.96	11.14	1.28
0.03	0.05	10	1	87.49	77.96	10.89	0.27
0.03	0.05	20	1	85.50	77.96	8.82	2.33

Table 7. Validation of FEM Analyzes

Tool corner radius (mm)	Depth of Cut, ap (mm)	Feed, f (mm/rev)	Cutting Speed, v (m/min)	Cutting force Experimental (Yağmur et al., 2021) (N)	Cutting force FEM (N)	Validation ratio (%)	
0.4	0.26	0.14	200	82.40	74.84	90.83	
			400	65.56	71.94	91.13	
	0.8		200	96.61	90.62	93.80	
			400	77.96	85.50	91.18	

RESULTS AND DISCUSSION

According to FEM analysis, variations of cutting force are given in Figure 3, and variations of cutting power are shown in Fig. 4 for all cutting depths and all machining parameters. When Figures 3 and 4 are examined, it has been observed that as the feed increased for all cutting depths, the cutting forces and cutting power also increased. This phenomenon is a result of the rise in cutting zone area as the feed increases (Gürbüz, Kafkas, and Şeker, 2012). During machining, an increase in cutting speed results in higher cutting zone temperatures, a reduction in the coefficient of friction, a decrease in the shear strength of the material in the second deformation zone, and a smaller tool-chip contact area. For these reasons, a decrease in cutting forces is an expected result in machining operations (Gürbüz, Şeker, and Kafkas, 2020; Ciftci, 2006; Zhao, Ai, and Li, 2006). However, upon examining Fig. 3, it is evident that the effect of increasing cutting speed on cutting forces was not significant. It is believed that the increase in cutting speed led to a rise in contact length, which in turn increased the cutting forces. For further clarification on this case, Figure 5 displays the impact of changes in cutting speed on the cutting zone temperature, pressure, and Von Mises stresses while maintaining the same cutting parameters. When Figure 5 is examined, it is understood that the cutting zone temperatures at 900m/min cutting speed were higher than that at 300m/min. Similarly, the cutting zone pressure and Von Mises stress increased at 900m/min cutting speed. For these reasons, it can be justified that increase in temperature reduced the shear strength, and the increase in contact length raised the cutting force. When Figure 4 is examined, it is seen that the cutting power raised significantly with the increase in cutting speed. This rise in cutting power may explain the unexpected behavior in cutting forces. The lowest cutting forces were obtained at cutting depth of 0.3 mm and feed of 0.1 mm/rev in all machining parameters (Fig. 3). The lowest power consumption was obtained with 300 m/min cutting speed at cutting depth of 0.3 mm and feed of 0.1 mm/rev (Fig. 4).

Variance and regression analysis were made by assuming that the cutting forces and cutting power findings obtained from FEM analyses vary according to independent control factors (cutting depth, cutting speed and feed). P values in statistical analyses were generally less than 5% ($P < 0.05$). A value of 0.549 was obtained only for the cutting speed factor in the cutting force analysis (Table 8). This is thought to be caused by the effect of the inconsistency between cutting speed and contact length on the cutting force (Fig. 3 and 4). Low P values obtained from other independent control factors indicate that the control factor and level selection are statistically significant (Bolar et al., 2018; Yılmaz et al., 2014). When Table 8 is examined, it is seen that the most effective control factor on the cutting force

was the cutting depth with a percent contribution of 91.74%, and the most effective control factor on the cutting power was the cutting speed with a percent contribution of 33.13%.

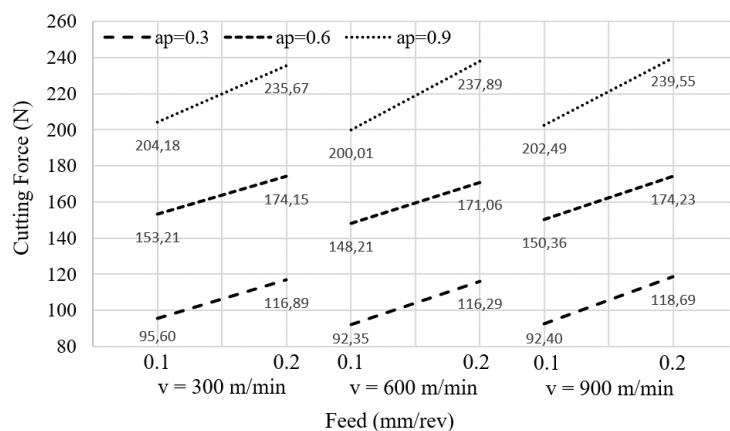


Figure 3. Cutting Force Variations at Different Machining Conditions based on the Cutting Depth

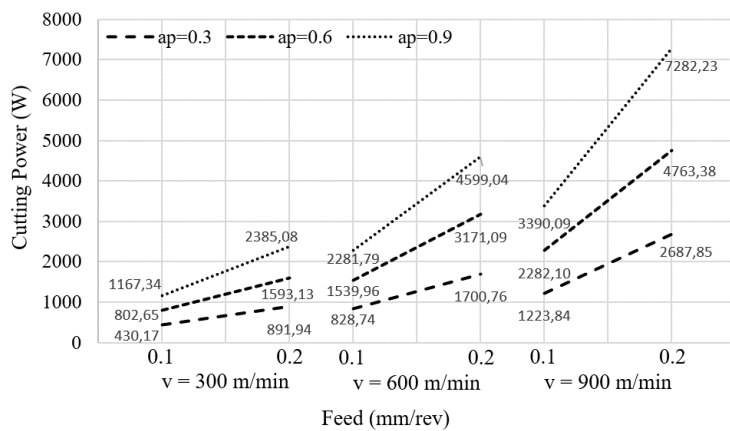


Figure 4. Cutting Power Variations at Different Machining Conditions based on the Cutting Depth

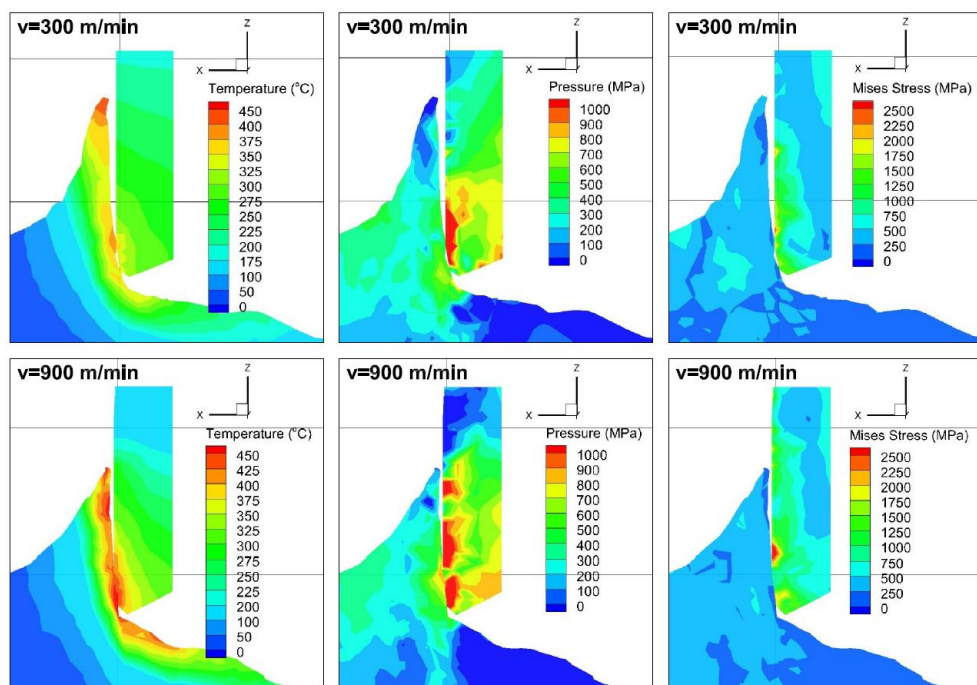
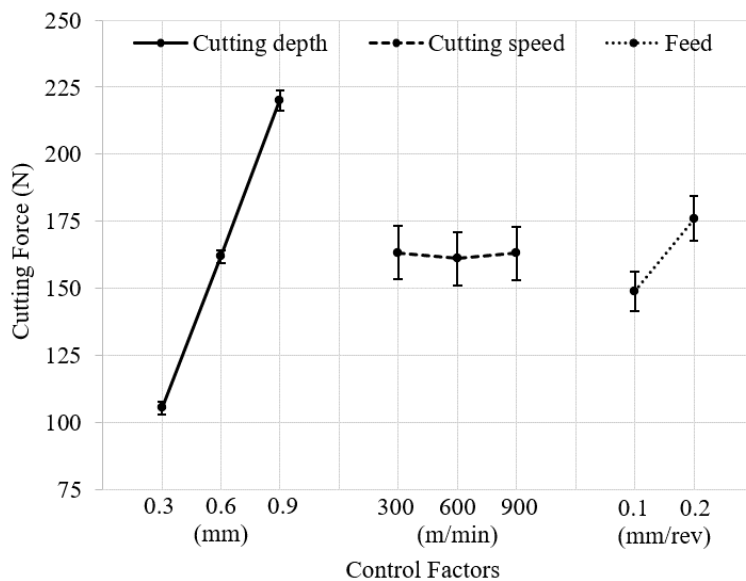


Figure 5. Cutting Temperature, Pressure and Von Mises Stress Distributions at $ap=0.3$ mm and $f=0.2$ mm/rev
Machining Parameters depending on Cutting Speed

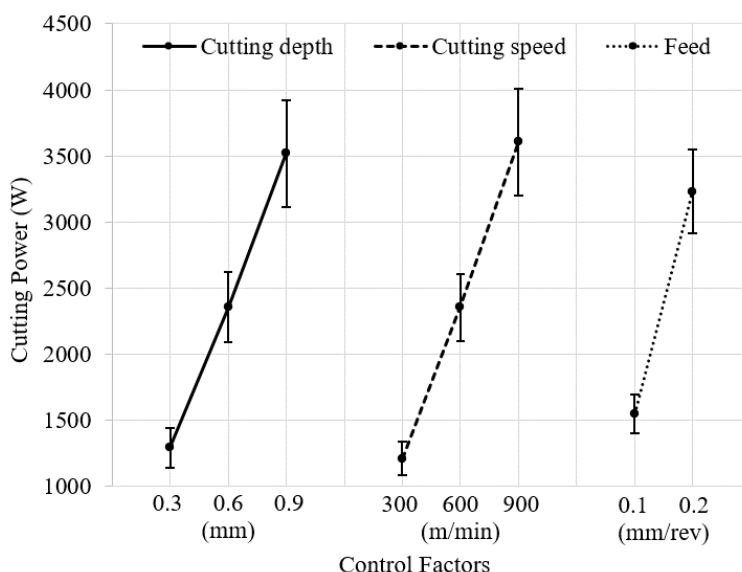
Table 8. ANOVA Results

Source	DF	Adj-SS	Adj-MS	F-value	P-value	Contribution (%)
<i>Cutting force (N)</i>						
<i>Linear model</i>	5	42769	8553.8	574.09	0.000	99.58
<i>Cutting depth, ap</i>	2	39398.6	19699.3	1322.12	0.000	91.74
<i>Cutting speed, v</i>	2	18.8	9.4	0.63	0.549	0.04
<i>Feed, f</i>	1	3351.6	3351.6	224.94	0.000	7.80
<i>Error</i>	12	178.8	14.9			0.42
<i>Total</i>	17	42947.8				100.00
<i>Cutting power (W)</i>						
<i>Linear model</i>	5	44751617	8950323	15.03	0.000	86.23
<i>Cutting depth, ap</i>	2	14843502	7421751	12.46	0.001	28.60
<i>Cutting speed, v</i>	2	17194164	8597082	14.43	0.001	33.13
<i>Feed, f</i>	1	12713951	12713951	21.35	0.001	24.50
<i>Error</i>	12	7147223	595602			13.77
<i>Total</i>	17	51898841				100.00

In order to see the behaviors of the responses as a result of the variation of machining parameters (control factors) more clearly, the impact graphs are given in Figure 6 and Figure 7. In the graphs, cutting force, cutting power values, and their standard errors are given for each level of each independent control factor. The impact plots were created by calculating the average of the dependent variables (Y-axis) obtained by using whichever control factor (X-axis) effect is desired to be shown. For example, to show the effect of the cutting depth factor on the cutting force, the cutting force values obtained by using for example a cutting depth of 0.3 mm are gathered, the average of these force values is calculated and then marked on the graph for this cutting depth, and all the graphs are generated continuing in this way. When Figure 6 is examined, it is seen that the cutting force raised with the increased cutting depth and feed. It is understood that the cutting speed parameter did not have a significant effect on the cutting force as discussed earlier (Figure 3). When Figure 7 is examined, it is observed that the cutting power raised with the increase in cutting depth, cutting speed, and feed. When the standard errors are examined, it is obtained that all levels of the cutting speed factor had coincident domains in terms of cutting force (Figure 6). It is understood that there were independent domains of influence in terms of cutting force and cutting power for all levels of other factors (Figures 6 and 7).

**Figure 6.** Impact Graphs depending on the Cutting Force

The model summary obtained by regression analyzes is given in Table 9. The coefficients of determination (R^2) of the statistical model were found to be 99.53% for cutting force and 86.19% for cutting power. These ratios indicate that the statistical models established with the FEM analyses are compatible and the results are consistent. The regression equations are shown in Eq. 4 for cutting force and Eq. 5 for cutting power.

**Figure 7.** Impact Graphs depending on the Cutting Power**Table 9.** Summary of Statistical Models

S	R ²	R ² (adj)	R ² (pred)
<i>Cutting force</i>			
3.778	99.53%	99.44%	99.23%
<i>Cutting power</i>			
715.545	86.19%	82.23%	74.44%

$$\text{Cutting force} = 7.20 + (57.30 \times ap) - (0.16 \times v) + (27.29 \times f) \quad (4)$$

$$\text{Cutting power} = -4748 + (1112 \times ap) + (1197 \times v) + (1681 \times f) \quad (5)$$

CONCLUSION

In this study, machining behaviors of AA6082-T4 alloy in terms of cutting forces and cutting power using cutting depth smaller than the tool corner radius and different machining parameters were investigated when performing a turning operation with PCD insert. In this context, FEM analyses followed by variance and regression analyses were performed by choosing different cutting depths, cutting speeds, and feeds. The conclusions drawn from the findings are presented below:

- In terms of cutting force; it was understood that the cutting forces were reduced at smaller cutting depths and lower feeds. The lowest cutting forces were obtained at cutting depth of 0.3 mm and feed of 0.1 mm/rev.
- It was observed that the cutting forces remained largely unchanged despite variations in the cutting speed. It is thought that this situation is caused by a compensation phenomenon in which the increasing chip length conceals the effect of decreasing shear strength in the flow zone at higher cutting speeds.
- In terms of cutting power; it was concluded that power consumption reduced with decreasing cutting depth, cutting speed, and feed. The lowest cutting power was obtained at cutting speed of 300 m/min, cutting depth of 0.3 mm, and feed of 0.1 mm/rev.
- In terms of variance and regression analysis; it was concluded that the most effective machining parameters were the cutting depth with a ratio of 91.74% for the cutting force and the cutting speed with a ratio of 33.13% for the cutting power. As a result of obtaining the coefficients of determination of the statistical model as 99.53% for the cutting force and 86.19% for cutting power, it was understood that statistical models were able to describe the variance in cutting force and cutting power values calculated by FEM analyses.
- As a result of validating the FEM analyses with the experimental measurements in the literature with a rate of over 90%, an acceptable Johnson-Cook material model for AA6082-T4 aluminum alloy for future studies was created.

As a result, the effects of different machining conditions on the cutting force and cutting power were determined for machining operations where the cutting depth is preferred smaller than the tool corner radius in order to achieve high surface quality in the machining of AA6082-T4 alloy. In addition, the Johnson-Cook material model of AA6082-T4 alloy has been added to the literature especially for use in machining operations.

REFERENCES

- AdvantEdge. (2015). *AdvantEdge 7.1 User's Manual*. Minneapolis, USA: Third Wave Systems.
- Bolar, G., Das, A., & Joshi, S. N. (2018). Measurement and analysis of cutting force and product surface quality during end-milling of thin-wall components. *Measurement*, 121, 190-204.
- Børvik, T., Olovsson, L., Dey, S., & Langseth, M. (2011). Normal and oblique impact of small arms bullets on AA6082-T4 aluminium protective plates. *International Journal of Impact Engineering*, 38(7), 577-589.
- Campatelli, G., & Scippa, A. (2012). Prediction of milling cutting force coefficients for Aluminum 6082-T4. *Procedia CirP*, 1, 563-568.
- Chandrasekaran, V. V., & Payton, L. N. (15-21 November 2013). *Comparison orthogonal tube turning data versus finite element simulation using LS Dyna*. Paper presented at the ASME International Mechanical Engineering Congress and Exposition, California, USA.
- Ciftci, I. (2006). Machining of austenitic stainless steels using CVD multi-layer coated cemented carbide tools. *Tribology International*, 39(6), 565-569. doi:<https://doi.org/10.1016/j.triboint.2005.05.005>
- Çiftçi, İ., & Gökçe, H. (2019). Molibden alaşımının işlenmesinde kesici takım ve kesme parametrelerinin Taguchi Metodu ile optimizasyonu. *Journal of the Faculty of Engineering and Architecture of Gazi University*, 34(1).
- Dandekar, C. R., Shin, Y. C., & Barnes, J. (2010). Machinability improvement of titanium alloy (Ti-6Al-4V) via LAM and hybrid machining. *International Journal of Machine Tools and Manufacture*, 50(2), 174-182.
- Davim, J. P., Maranhao, C., Jackson, M., Cabral, G., & Gracio, J. (2008). FEM analysis in high speed machining of aluminium alloy (Al7075-0) using polycrystalline diamond (PCD) and cemented carbide (K10) cutting tools. *The International Journal of Advanced Manufacturing Technology*, 39(11-12), 1093-1100.
- Davim, J. P., Reis, P., Maranhao, C., Jackson, M., Cabral, G., & Gracio, J. (2010). Finite element simulation and experimental analysis of orthogonal cutting of an aluminium alloy using polycrystalline diamond tools. *International Journal of Materials and Product Technology*, 37(1-2), 46-59.
- Davoudinejad, A., Doagou-Rad, S., & Tosello, G. (2018). A finite element modeling prediction in high precision milling process of aluminum 6082-T6. *Nanomanufacturing and Metrology*, 1(4), 236-247.
- DTS. Diamond Indexable Inserts. Retrieved from https://en.diamond-toolingsystems.com/wp-content/uploads/2021/11/01_Diamond-Inserts-Catalog_DTSGmbH.pdf
- El-Danaf, E. A., AlMajid, A. A., & Soliman, M. S. (2008). Hot deformation of AA6082-T4 aluminum alloy. *Journal of materials science*, 43(18), 6324-6330.
- Eurocode. (2007). 9: Design of Aluminium Structures-Part 1-1: General Structural Rules. European Committee for Standardization. In. Brussels, Belgium: CEN, EN 1999-1-1: 2007.
- Gao, G., Wu, B., Zhang, D., & Luo, M. (2013). Mechanistic identification of cutting force coefficients in bull-nose milling process. *Chinese Journal of Aeronautics*, 26(3), 823-830.
- Gurusamy, M., & Sriram, S. (2022). Investigations on the Choice of Johnson–Cook Constitutive Model Parameters for the Orthogonal Cutting Simulation of Inconel 718. *Journal of Advanced Manufacturing Systems*, 1-25.
- Gürbüz, H., Kafkas, F., & Şeker, U. (2012). AISI 316L eğeliğinin işlenmesinde kesici takım kesici kenar formu ve talaş kırıcı formlarının kesme kuvvetleri ve yüzey pürüzlülüğü üzerine etkisi. *Batman Üniversitesi Yaşam Bilimleri Dergisi*, 1(2), 173-184.
- Gürbüz, H., Şeker, U., & Kafkas, F. (2020). Effects of cutting tool forms on the surface integrity in turning of AISI 316L stainless steel. *Journal of the Faculty of Engineering and Architecture of Gazi University*, 35(1), 225-240. doi:<https://doi.org/10.17341/gazimmfd.454386>

- Hasçelik, A., & Aslantaş, K. (2021). Mikro Tornalama İşleminde Kesici Takım Burun Yarıçapının Kesme Kuvvetlerine Etkisi. *Journal of Materials and Mechatronics: A*, 2(1), 13-25.
- Hazır, E., Erdinler, E. S., & Koc, K. H. (2018). Optimization of CNC cutting parameters using design of experiment (DOE) and desirability function. *Journal of Forestry Research*, 29(5), 1423-1434.
- Jaspers, S., & Dautzenberg, J. (2002). Material behaviour in conditions similar to metal cutting: flow stress in the primary shear zone. *Journal of Materials Processing Technology*, 122(2-3), 322-330.
- Karahan, B., İnce, U., Yurdas, S., Kilinçdemir, N. E., Ağarer, F. C., & Kılıçaslan, C. (29-30 September 2017). *On the Cold Forging of 6082 H13 and T4 Aluminum Alloy Bushes*. Paper presented at the 5th International Symposium on Innovative Technologies in Engineering and Science, Baku, Azerbaijan.
- Kumar, S. L. (2018). Experimental investigations and empirical modeling for optimization of surface roughness and machining time parameters in micro end milling using Genetic Algorithm. *Measurement*, 124, 386-394.
- Mamedov, A., & Lazoglu, I. (2013). Machining forces and tool deflections in micro milling. *Procedia CirP*, 8, 147-151.
- Mazzolani, F. (1994). *Aluminium alloy structures*. London, UK: CRC Press.
- Ozlu, B., & Ugur, L. (2021). Optimization of cutting forces on turning of Ti-6Al-4V Alloy by 3D FEM simulation analysis. *Journal of Engineering Research and Applied Science*, 10(2), 1789-1795.
- Rao, B., Dandekar, C. R., & Shin, Y. C. (2011). An experimental and numerical study on the face milling of Ti-6Al-4V alloy: Tool performance and surface integrity. *Journal of Materials Processing Technology*, 211(2), 294-304.
- Shetty, R., Kumar, S., Mallagi, R., & Keni, L. (2021). L 1 6 Orthogonal Array-Based Three-Dimensional Finite Element Modeling for Cutting Force and Chip Formation Analysis During Dry Machining of Ti-6Al-4V. *Journal of Advanced Manufacturing Systems*, 20(01), 123-134.
- Spigarelli, S., Evangelista, E., & McQueen, H. (2003). Study of hot workability of a heat treated AA6082 aluminum alloy. *Scripta Materialia*, 49(2), 179-183.
- Stanojković, J., & Radovanović, M. (2017). Selection of solid carbide end mill for machining aluminum 6082-T4 using mcdm method. *University Politehnica of Bucharest Scientific Bulletin Series D*, 79(1), 175-184.
- Torić, N., Brnić, J., Boko, I., Brčić, M., Burgess, I. W., & Uzelac, I. (2017). Experimental analysis of the behaviour of aluminium alloy EN 6082AW T6 at high temperature. *Metals*, 7(4), 126.
- Uğur, L. (2022). A Numerical and Statistical Approach of Drilling Performance on Machining of Ti-6Al-4V Alloy. *Surface Review and Letters*, 29(12), 2250168-2250137.
- Uğur, L., Kazan, H., & Özlü, B. (2022). Investigation of the Impacts of Cutting Parameters on Power Usage in Cryogenic-Assisted Turning of AISI 52100 Bearing Steel by FEM. *İmalat Teknolojileri ve Uygulamaları*, 3(3), 55-61.
- Yadav, R. N. (2021). Statistical and Intelligent Techniques for Modeling and Optimization of Duplex Turning for Aerospace Material. *Journal of Advanced Manufacturing Systems*, 20(02), 341-367.
- Yağmur, S., Kaya, M., & Şeker, U. (7-9 Kasım 2019). *PCD Takımlarda Farklı Talaş Kirıcı Formlarının AA6082 T4 Alaşımının Yüzey Pürüzlülüğüne Etkisi*. Paper presented at the 10th International Congress on Machining, Antalya, Turkey.
- Yağmur, S., Kaya, M. K., & Şeker, U. (2021). AA-6082 T4 Alaşımının Tornalamasında Çok Kristalli Elmas (ÇKE) Takımlara Uygulanan Talaş Kirıcı Formlarının Kesme Kuvvetleri Üzerindeki Etkilerinin Araştırılması. *Gazi Mühendislik Bilimleri Dergisi*, 7(1), 51-57.
- Yılmaz, V., Dilipak, H., Sarıkaya, M., Yılmaz, C. Y., & Özdemir, M. (2014). Frezeleme işlemlerinde kesme kuvveti, titreşim ve yüzey pürüzlülüğü sonuçlarının modellenmesi. *Erciyes Üniversitesi Fen Bilimleri Enstitüsü Fen Bilimleri Dergisi*, 30(4), 220-226.
- Zhao, J., Ai, X., & Li, Z. L. (2006). *Finite element analysis of cutting forces in high speed machining*. Paper presented at the Materials Science Forum, Switzerland.